Intersubunit conformational changes mediate epithelial sodium channel gating

Daniel M. Collier,[1,2] Vivian R. Tomkovicz,[1,2] Zerubbabel J. Peterson,[1,2] Christopher J. Benson,[1,3] and Peter M. Snyder[1,2,3]

[1]Department of Internal Medicine and [2]Department of Molecular Physiology and Biophysics, University of Iowa Carver College of Medicine, Iowa City, IA 52242

[3]Iowa City VA Health Care System, Iowa City, IA 52246

The epithelial Na^+ channel (ENaC) functions as a pathway for Na^+ absorption in the kidney and lung, where it is crucial for Na^+ homeostasis and blood pressure regulation. However, the basic mechanisms that control ENaC gating are poorly understood. Here we define a role in gating for residues forming interfaces between the extracellular domains of the three ENaC subunits. Using cysteine substitution combined with chemical cross-linking, we determined that residues located at equivalent positions in the three subunits (α_{K477}, β_{E446}, and γ_{E455}) form interfaces with residues in adjacent subunits (β_{V85}, γ_{V87}, and α_{L120}, respectively). Cross-linking of these residues altered ENaC activity in a length-dependent manner; long cross-linkers increased ENaC current by increasing its open probability, whereas short cross-linkers reduced ENaC open probability. Cross-linking also disrupted ENaC gating responses to extracellular pH and Na^+, signals which modulate ENaC activity during shifts in volume status. Introduction of charged side chains at the interfacing residues altered ENaC activity in a charge-dependent manner. Current increased when like charges were present at both interfacing residues, whereas opposing charges reduced current. Together, these data indicate that conformational changes at intersubunit interfaces participate in ENaC transitions between the open and closed states; movements that increase intersubunit distance favor the open state, whereas the closed state is favored when the distance is reduced. This provides a mechanism to modulate ENaC gating in response to changing extracellular conditions that threaten Na^+ homeostasis.

The Journal of General Physiology

INTRODUCTION

The epithelial Na^+ channel (ENaC), a heterotrimer of α, β, and γ subunits, functions as a pathway for Na^+ absorption across epithelia in the kidney collecting duct and connecting tubule, lung, distal colon, and sweat duct (Schild, 2004; Snyder, 2005). In this role, the channel is critical for the maintenance of extracellular Na^+ and volume balance. ENaC mutations and defects in its regulation cause inherited forms of hypertension (e.g., Liddle's syndrome) and hypotension (pseudohypoaldosteronism type 1; Lifton, 1996) and may contribute to the pathogenesis of lung disease in cystic fibrosis (Boucher et al., 1986). ENaC is a member of the degenerin (DEG)/ENaC family of cation channels, which share common structural features, including two transmembrane domains, relatively short cytoplasmic amino and carboxy termini, and a large highly structured extracellular domain (Ben-Shahar, 2011).

ENaC gating is modulated by a variety of extracellular signals. In the kidney collecting duct, the Na^+ and Cl^- concentrations vary widely, decreasing to <10 mM under conditions of hypovolemia and increasing to >150 mM with volume excess (Rose, 1984). Both Na^+ and Cl^- inhibit ENaC activity ("Na^+ self-inhibition" and "Cl^- inhibition"), functioning as negative feedback mechanisms to reduce Na^+ absorption (Garty and Palmer, 1997; Chraïbi and Horisberger, 2002; Sheng et al., 2004; Collier and Snyder, 2009a, 2011). Serine proteases enhance ENaC activity by removing inhibitory fragments from the extracellular domains of the α and γ subunits (Hughey et al., 2003, 2004; Caldwell et al., 2004; Carattino et al., 2008; Kashlan et al., 2012). Laminar sheer stress stimulates ENaC under conditions of increased urine flow (Carattino et al., 2004; Morimoto et al., 2006). ENaC is also exposed to wide fluctuations in extracellular pH. Urine pH varies from 4.5 to 8, becoming acidic in response to hypovolemia and alkaline with hypervolemia (Rose, 1984). Urine pH also varies with diet and with metabolic acidosis and alkalosis. In the lung, airway surface liquid is slightly alkaline (pH 7.8–8.1) but becomes acidic with lung diseases including pneumonia and cystic fibrosis (Hunt, 2007; Pezzulo et al., 2012). Changes in pH within these ranges modulate ENaC gating; acidic pH stimulates ENaC, whereas alkaline pH inhibits ENaC (Collier and Snyder, 2009b).

Correspondence to Peter M. Snyder: peter-snyder@uiowa.edu

Abbreviations used in this paper: DEG, degenerin; DTT, dithiothreitol; ENaC, epithelial Na^+ channel.

The Rockefeller University Press $30.00
J. Gen. Physiol. Vol. 144 No. 4 337–348
www.jgp.org/cgi/doi/10.1085/jgp.201411208

Although changes in ENaC gating are critical for regulating epithelial Na^+ transport, the basic mechanisms that control ENaC opening and closing are poorly understood. However, there are some recent data to guide us. Crystallization of a related DEG/ENaC ion channel (cASIC1a) in desensitized (Jasti et al., 2007; Gonzales et al., 2009) and toxin-bound (Baconguis and Gouaux, 2012; Dawson et al., 2012; Baconguis et al., 2014) states has facilitated the generation of ENaC structural models, and mutagenesis has begun to identify residues necessary for regulation of ENaC gating. In the current work, we explore the mechanisms that underlie gating by taking advantage of extracellular domain residues located at an equivalent position in the three ENaC subunits. βENaC-E446 and γENaC-E455 function as putative proton sensors; mutation of these residues reduced ENaC activation by acidic pH (Collier et al., 2012). In contrast, the equivalent residue in αENaC (K477) carried a positive charge and its mutation enhanced acid activation of ENaC (Collier et al., 2012). Here we demonstrate that these residues are located at intersubunit interfaces, where they participate in conformational changes required for ENaC to transition between open and closed states.

MATERIALS AND METHODS

DNA constructs

cDNAs for human α-, β-, and γENaC in pMT3 were cloned as previously described (McDonald et al., 1994, 1995). Mutations were generated by site-directed mutagenesis (QuikChange II XL; Agilent Technologies) and sequenced in the University of Iowa DNA Core.

Homology modeling and molecular graphics

A model of αβγENaC based on the chicken ASIC1 crystal structure (PDB ID 4NYK) was generated using Phyre2 (Kelley and Sternberg, 2009). Structures of each subunit were aligned to the appropriate subunit of the ASIC1a homotrimer using UCSF Chimera. Molecular graphics and analyses were performed with the UCSF Chimera package (Resource for Biocomputing, Visualization, and Informatics, University of California, San Francisco, supported by NIGMS P41-GM103311; Pettersen et al., 2004).

Biochemical cross-linking

HEK 293T cells cultured in Dulbecco's modified Eagle's medium (DMEM) were transfected with cDNAs encoding human α-, β-, and γENaC using Lipofectamine 2000 (Invitrogen). After transfection, 10 µM amiloride was added to the culture medium. To reduce spontaneous disulfide bonds, cells were incubated with 50 mM dithiothreitol (DTT) for 15 min at 37°C in Ringer's solution (135 mM NaCl, 1.2 mM $CaCl_2$, 1.2 mM $MgCl_2$, 2.4 mM K_2HPO_4, 0.6 mM KH_2PO_4, and 10 mM HEPES, pH 7.4) with 10 µM amiloride. To cross-link cysteines, cells were treated with MTS reagents (100 µM MTS-14-O4-MTS or MTS-2-MTS [Toronto Research Chemicals]) or vehicle (DMSO) at room temperature for 30 s (or 5 min for $\alpha\beta_{E446C}\gamma_{V87C}$) in Ringer's solution with 10 µM amiloride.

To label and isolate cell surface ENaC, cells were washed with ice-cold PBS with 1 mM $CaCl_2$ and $MgCl_2$ (PBS-CM), labeled with 0.5 mg/ml sulfo-NHS-biotin (Thermo Fisher Scientific) in PBS-CM for 20 min on ice, and quenched by incubation with 100 mM glycine in PBS-CM for 10 min. After washing three times with PBS-CM, cells were lysed in 0.4% sodium deoxycholate, 1% Nonidet P-40, 63 mM EDTA, 50 mM Tris-HCl, pH 8, protease inhibitor mixture (Sigma-Aldrich), and 30 mM *N*-ethylmaleimide (Sigma-Aldrich). Biotin-labeled cell surface proteins were isolated by incubating 500 µg of cell lysate with immobilized NeutrAvidin beads (Thermo Fisher Scientific) for 12 h at 4°C, and ENaC subunits were detected by immunoblotting using anti-β or anti-γ polyclonal antibody (1:2,000; StressMarq) followed by incubation with anti–rabbit IgG antibody-peroxidase conjugate (1:2,000; Santa Cruz Biotechnology, Inc.) and enhanced chemiluminescence (ECL 2; Thermo Fisher Scientific). Total ENaC was detected by immunoblotting of the cell lysate (25 µg).

Expression and whole-cell electrophysiology in *Xenopus laevis* oocytes

Oocytes were harvested from albino *Xenopus* females and manually defolliculated after a 1-h treatment with 2.4 U FALGPA activity per milliliter of type IV collagenase (Worthington Biochemical Corporation) in Ca^{2+}-free ND-96 (96 mM NaCl, 2 mM KCl, 1 mM $MgCl_2$, and 5 mM HEPES, pH adjusted to 7.4 with NaOH). After nuclear injection of cDNAs encoding α-, β-, and γENaC (0.02 µg/µl each), cells were incubated at 18°C in modified Barth's saline (88 mM NaCl, 1 mM KCl, 0.33 mM $Ca(NO_3)_2$, 0.41 mM $CaCl_2$, 0.82 mM $MgSO_4$, 2.4 mM $NaHCO_3$, 10 mM HEPES, 50 µg/ml gentamicin sulfate, 10 µg/ml sodium penicillin, and 10 µg/ml streptomycin sulfate, pH adjusted to 7.4 with NaOH) for 20–24 h before study. Oocytes were voltage clamped to −60 mV (two-electrode voltage clamp), and currents were amplified with an Oocyte Clamp OC-725C (Warner Instruments), digitized with a MacLab/200 interface (ADInstruments), and recorded and analyzed with Chart software (ADInstruments). Cells were bathed in 116 mM NaCl, 2 mM KCl, 0.4 mM $CaCl_2$, 1 mM $MgCl_2$, and 5 mM HEPES, pH adjusted to 7.4 with NaOH. Cysteines were modified by treatment with MTS reagents (100 µM for 30 s; MTS-2-MTS, 1,2-ethanediyl bis-MTS; MTS-4-MTS, 1,4-butanediyl bis-MTS; MTS-6-MTS, 1,6-hexanediyl bis-MTS; MTS-11-O3-MTS, 3,6,9-trioxaundecane-1,11-diyl-bis-MTS; MTS-14-O4-MTS, 3,6,9,12-tetraoxatetradecane-1,14-diyl-bis-MTS; MTSES, sodium (2-sulfonatoethyl)MTS; MTSET, [2-(trimethylammonium)ethyl]MTS bromide) or reduced with DTT (30 mM for 30 s). ENaC current was determined by addition of 10 µM amiloride to the bathing solution. To quantitate Na^+ self-inhibition, cells were bathed in low sodium (1 mM NaCl, 115 mM *N*-methyl-D-glucamine, 2 mM KCl, 0.4 mM $CaCl_2$, 1 mM $MgCl_2$, and 5 mM HEPES, pH adjusted with HCl) and then rapidly shifted to high sodium (116 mM NaCl). Na^+ self-inhibition was quantitated as [(peak current − steady-state current)/peak current]. pH responses were measured in low Cl^- bath solution (58 mM Na_2SO_4, 58 mM D-mannitol, 2 mM KCl, 0.4 mM $CaCl_2$, 1 mM $MgCl_2$, and 5 mM HEPES, pH adjusted with NaOH).

Single-channel studies in *Xenopus* oocytes

ENaC was expressed in *Xenopus* oocytes by cytoplasmic injection of equal concentrations of α-, β-, and γENaC cRNA (1 µg/µl each) generated by in vitro transcription using mMessage mMachine T7 (Ambion). Injection volumes were varied between ∼5 and 20 nl to titrate ENaC expression to optimize the likelihood of recording from patches containing only one to three channels. Single-channel currents were recorded from devitellinized oocytes in the cell-attached patch-clamp configuration 1–3 d after injection. The pipette solution contained 110 mM LiCl, 2 mM KCl, 1.54 mM $CaCl_2$, and 10 mM HEPES, pH 7.4 with LiOH; or 1 mM LiCl, 109 mM NMDG, 2 mM KCl, 1.54 mM $CaCl_2$, and 10 mM HEPES, pH 7.4 with HCl. In all experiments, the bath solution contained 110 mM LiCl, 2 mM KCl, 1.54 mM $CaCl_2$, 10 mM HEPES, pH 7.4 with LiOH. Li^+ was used in place of Na^+ to increase the signal to noise ratio. Currents were amplified using an Axopatch 200B amplifier (Axon Instruments), acquired at 4 kHz and filtered with a 1-kHz

Bessel filter, and stored using Pulse software (version 8.53; HEKA). Currents were digitally filtered at 50 Hz, and amplifier artifacts were removed for analysis. Currents were analyzed using TAC (version 3.0.8; Bruxton Corporation). Slope conductance was determined between −100 and −40 mV. Open state probability (P_O) was determined from recordings of patches containing one to three channels for 5–10-min duration (−100 mV for inward current and 60 mV for outward current). The number of channels per patch was estimated by counting current levels. The majority of patches contained one to two channels. To study the effects of modification with MTS compounds, cells were pretreated with the MTS compound before seal formation.

Statistics

All data are expressed as mean ± SEM. Differences were assessed by paired or unpaired *t* tests, with significance indicated by $P < 0.05$.

RESULTS

Localization of intersubunit interfaces

We hypothesized that α_{K477}, β_{E446}, and γ_{E455} participate in conformational changes that underlie ENaC gating. To pursue this hypothesis, we first examined their locations in the ENaC channel complex. Fig. 1 A shows a partial sequence alignment of the three homologous ENaC subunits and ASIC1a; α_{K477}, β_{E446}, and γ_{E455} are located between two cysteines that are conserved throughout the DEG/ENaC family of ion channels. Fig. 1 B shows a homology model of ENaC based on the crystal structure of ASIC1a (PDB ID 4NYK; Gonzales et al., 2009). The structure of a single subunit resembles the anatomy of a left hand. The region above the transmembrane domain is the wrist. The cysteine-rich region of the channel is the thumb. The central β-ball region sits within the palm domain, and the extremities of the structure are referred to as the knuckle and finger domains (Jasti et al., 2007). Our previous work indicates that the three ENaC subunits assemble in an αγβ orientation (listed clockwise) when viewing the channel from the extracellular side (Collier and Snyder, 2011). α_{K477}, β_{E446}, and γ_{E455} are located in a loop that connects the base of the thumb domain to the palm domain (Fig. 1 B). At this location, each residue is predicted to lie at an interface with its neighboring subunit. For example, β_{E446} is located at the interface with γENaC, close to γ_{V87} (Fig. 1 B). Likewise, α_{K477} is predicted to lie at an interface close to β_{V85}, and γ_{E455} at an interface with α_{L120} (Fig. 1 B). These three residues lie within the palm domain β1–β2 linker.

To begin to validate this model, we tested whether the putative pH-sensing residues at these potential interfaces could be chemically cross-linked to their predicted neighbors. We initially focused on the interface between α_{K477} and β_{V85}, replacing both residues with cysteine. After treatment with bifunctional cysteine-reactive compounds of differing lengths (MTS-x-MTS, where "x" indicates number of atoms in the linker backbone), we labeled and isolated ENaC at the cell surface by biotinylation, resolved ENaC on a nonreducing gel (to maintain subunit cross-linking), and then detected βENaC by immunoblot. With wild-type ENaC, we detected a band of ∼90 kD, corresponding to monomeric βENaC (Fig. 2 A). Treatment with MTS-14-O4-MTS or MTS-2-MTS did not alter migration of βENaC. This indicates that native cysteines are not sufficient to cross-link ENaC subunits. In contrast, when we expressed $\alpha_{K477C}\beta_{V85C}\gamma$ENaC, both MTS-14-O4-MTS and MTS-2-MTS induced appearance of a higher molecular mass band, corresponding to the predicted size for a β-α dimer (Fig. 2 A). Thus, α_{K477C} and β_{V85C} are located in close enough proximity to be cross-linked. The higher mass band was not present in the absence of cross-linker (DMSO), indicating that cross-links did not form spontaneously. As a control for specificity, we coexpressed β_{V85C} with γ_{E455C} (position equivalent

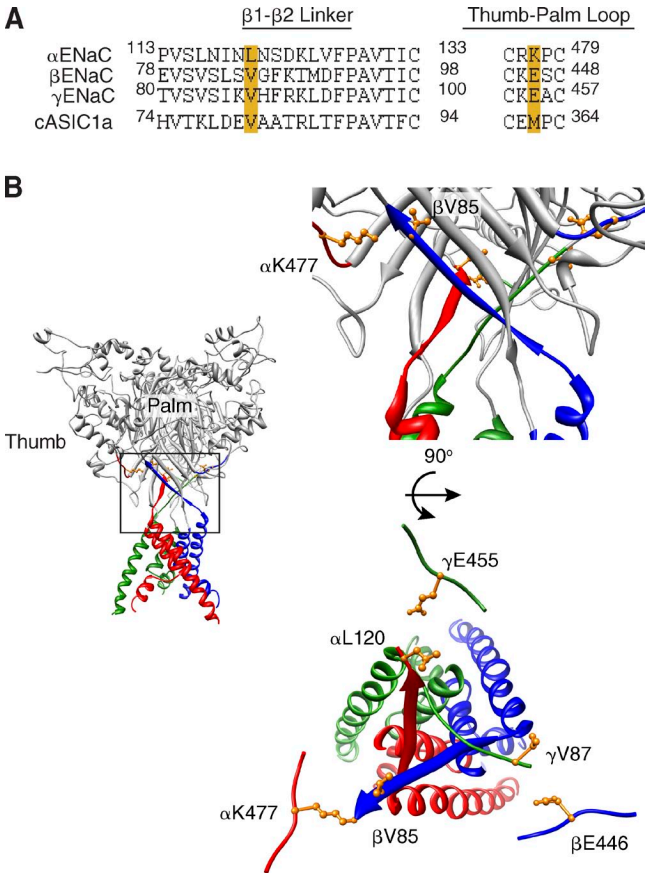

Figure 1. Extracellular intersubunit interfaces. (A) Partial sequence alignments of the extracellular domains of human α-, β-, and γENaC and chicken ASIC1a. Putative interfacing residues are indicated by gold boxes. (B) ENaC structural models: areas of interest in αENaC are shown in red, βENaC in blue, and γENaC in green. The structure on the left side shows membrane-spanning and extracellular domains. The right structures show close-up views (corresponding to the boxed portion of the left structure) from the side (top structure) and rotated 90° to view channel from the top (bottom structure). Side chains of putative interfacing residues are shown in orange. Some regions of the bottom structure are hidden for clarity.

to α_{K477C}). We did not detect cross-linking between these residues after MTS-14-O4-MTS treatment, consistent with the prediction that these residues are not located at the same interface (Fig. 2 A).

We performed similar experiments at the other two predicted intersubunit interfaces. With expression of $\alpha\beta_{E446C}\gamma_{V87C}$, MTS-14-O4-MTS and MTS-2-MTS induced cross-linking to form β-γ dimers (Fig. 2 B). However, with $\alpha_{L120C}\beta\gamma_{E455C}$ we detected a higher molecular mass band in the absence of cross-linking reagent (Fig. 2 C). This finding suggests that a spontaneous disulfide bond was formed between α_{L120C} and γ_{E455C}. Consistent with this possibility, the dimer band was abolished by the reducing agent DTT (Fig. 2 C). Together, the biochemical cross-linking data support the model that putative pH-sensing residues are located at interfaces with residues in the β1-β2 linkers of adjacent ENaC subunits (Fig. 1 B).

Cross-linking alters ENaC activity

If conformational changes at the intersubunit interfaces contribute to ENaC gating, then cross-linking might alter ENaC activity by introducing constraints to movement. We began by testing the effects of a long cross-linker, MTS-14-O4-MTS. In *Xenopus* oocytes expressing αβγENaC, we quantitated ENaC current using the open channel blocker amiloride (Fig. 3 A). We then treated the cells with MTS-14-O4-MTS in the continued presence of amiloride (to minimize modification of endogenous pore cysteines [Snyder et al., 1999]) and compared current after washout of MTS-14-O4-MTS and amiloride with current before treatment (Fig. 3, A, B, D, and E, blue lines). In cells expressing wild-type ENaC, MTS-14-O4-MTS produced a small (16.9 ± 3.1%) decrease in current (Fig. 3, A and C), likely by reacting with endogenous pore cysteines (Snyder et al., 1999). In contrast, when we expressed $\alpha_{K477C}\beta_{V85C}\gamma$ENaC, MTS-14-O4-MTS produced a large (421.4 ± 32.4%), irreversible increase in ENaC current (Fig. 3, B and C). This stimulation required cysteines at both positions; MTS-14-O4-MTS did not increase current when either cysteine was introduced individually (Fig. 3 C). The requirement for both cysteines indicates that simultaneous modification of both was required for ENaC stimulation, consistent with the formation of a cross-link between the residues. As an additional control for specificity, we introduced a cysteine at a neighboring position in βENaC (S84C). As part of a β sheet, its side chain is predicted to be in the opposite orientation as V85C. When we coexpressed β_{S84C} with α_{K477C} and γENaC, MTS-14-O4-MTS failed to stimulate ENaC current (Fig. 3 C).

We used the same strategy to examine the other two interfaces. At the interface between β_{E446C} and γ_{V87C},

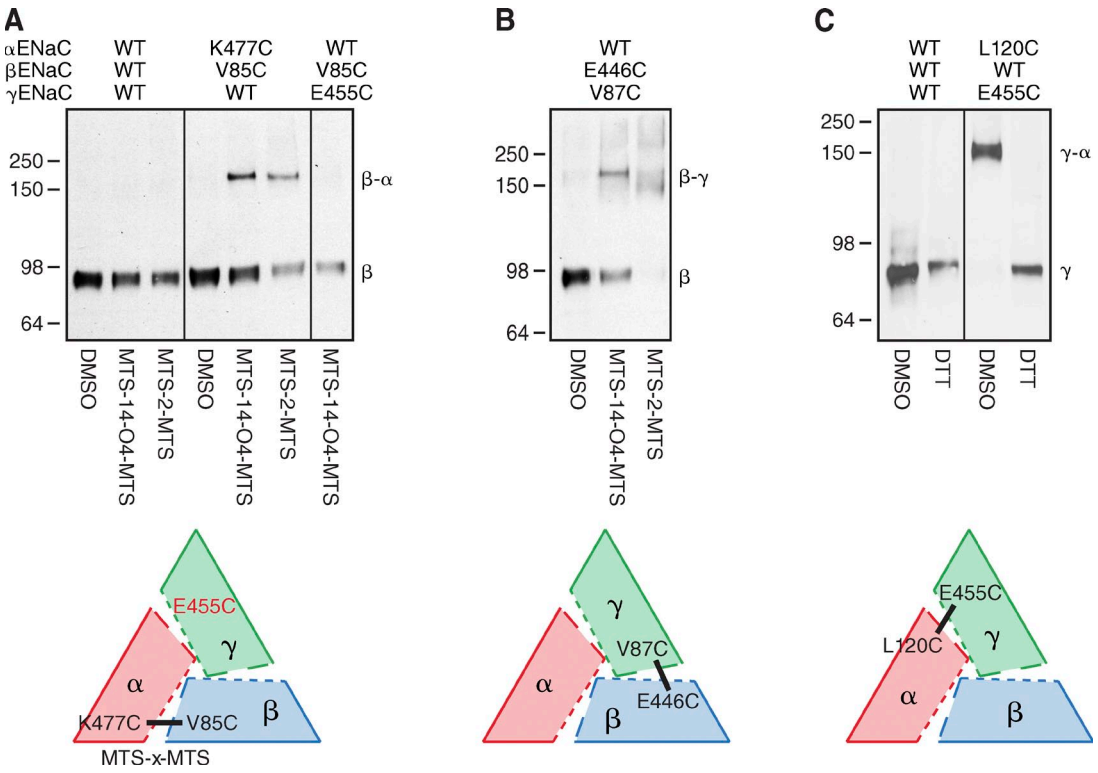

Figure 2. Cross-linking of intersubunit residues. (A–C) Representative immunoblots of βENaC (A and B) and γENaC (C) after isolation of the biotinylated cell surface fraction from HEK 293 cells expressing the indicated ENaC subunits. Cells were treated with DMSO (control), MTS-14-O4-MTS, MTS-2-MTS, or DTT, as indicated. Molecular mass is indicated in kilodaltons. Models illustrate the three ENaC subunits (viewed from the top) and locations of cross-linked residues.

cross-linking with MTS-14-O4-MTS increased current (28.9 ± 6.3%; Fig. 3, D and F), albeit to a lesser extent than its effect at the interface between α_{K477C} and β_{V85C}. At the interface between α_{L120C} and γ_{E455C} (which formed a spontaneous disulfide bond), MTS-14-O4-MTS also increased ENaC current (136.1 ± 12.8%; Fig. 3, E and F). Thus, a fraction of these channels likely lack spontaneous disulfide bonds, rendering them susceptible to cross-linking by MTS-14-O4-MTS. Together, the data lend additional support to a model in which α_{K477}, β_{E446}, and γ_{E455} are located at intersubunit interfaces with β_{V85}, γ_{V87}, and α_{L120}, respectively. Moreover, at each interface, cross-linking with MTS-14-O4-MTS increased ENaC current.

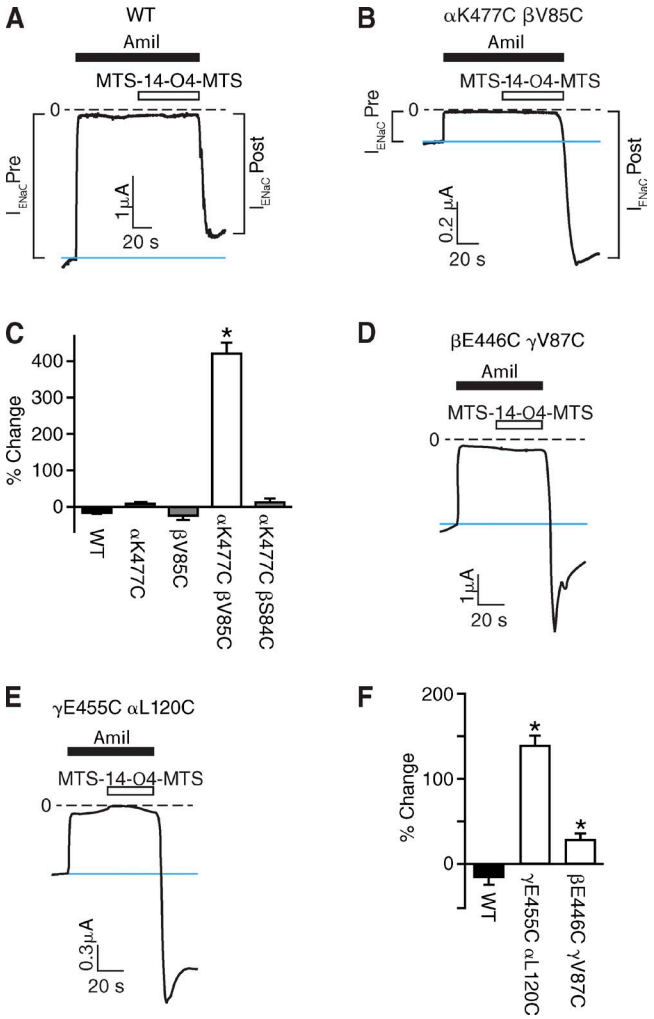

Figure 3. Cross-linking alters ENaC current. (A, B, D, and E) Representative current traces (voltage clamped to −60 mV) in oocytes expressing wild-type αβγENaC (A), $\alpha_{K477C}\beta_{V85C}\gamma$ENaC (B), $\alpha\beta_{E446C}\gamma_{V87C}$ENaC (D), and $\alpha_{L120C}\beta\gamma_{E455C}$ENaC (E). Records show ENaC current before (blue lines) and after treatment with MTS-14-O4-MTS (in the presence of amiloride [Amil]). (C and F) Percent change in ENaC current induced by MTS-14-O4-MTS in oocytes expressing αβγENaC (subunits are wild type or the indicated mutants). Mean ± SEM is shown (n = 6–12; *, $P < 0.001$).

Length dependence of cross-linking

To determine whether ENaC function is dependent on the distance between the residues at the intersubunit interface, we tested a range of different length cross-linkers. We focused on the interface between α_{K477} and β_{V85} because cross-linking at this location produced the largest effect on ENaC current. Fig. 4 shows the changes in ENaC current produced by cross-linkers ranging from 5.2 Å (MTS-2-MTS) to 20.8 Å (MTS-14-O4-MTS) in length (Loo and Clarke, 2001). When both α_{K477} and β_{V85} were replaced with cysteine, ENaC current was increased by MTS-14-O4-MTS and MTS-11-O3-MTS (Fig. 4). In contrast, shorter cross-linkers (MTS-6-MTS, MTS-4-MTS, and MTS-2-MTS) produced small decreases in ENaC current (Fig. 4). However, it is unclear whether they resulted from cross-linking of α_{K477} and β_{V85} because similar decreases were observed with wild-type ENaC or with single cysteine substitutions (with the exception of α_{K477C}, which was stimulated by MTS-2-MTS). Thus, the effect of cross-linking reagents on ENaC current was length dependent; only long reagents were sufficient to increase ENaC current. This suggests that an increase in intersubunit distance favors the open state.

As an additional test of this paradigm, we examined the functional effect of the spontaneous disulfide bond that formed at the interface between α_{L120C} and γ_{E455C} (Fig. 2 C). This bond constrains the interfacing residues in close proximity to one another. When we reduced this disulfide bond with DTT, there was a large increase in amiloride-sensitive current (Fig. 5, A and B). DTT produced a very small increase in current in cells expressing $\alpha\beta_{E446C}\gamma_{V87C}$ENaC, but had no effect on $\alpha_{K477C}\beta_{V85C}\gamma$ENaC or wild-type ENaC (Fig. 5 B). Thus, in contrast to the effect of long cross-linkers, shortening the distance between α_{L120C} and γ_{E455C} (by spontaneous disulfide bonding) inhibits ENaC activity. Together, the data support a model in which increased intersubunit distance favors

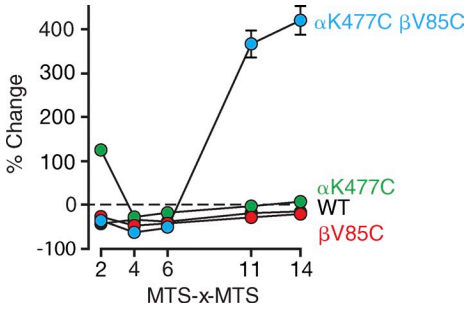

Figure 4. Length dependence of cross-linking. Percent change in ENaC current in *Xenopus* oocytes expressing αβγENaC (black), $\alpha_{K477C}\beta\gamma$ (green), $\alpha\beta_{V85C}\gamma$ (red), or $\alpha_{K477C}\beta_{V85C}\gamma$ENaC (blue) induced by treatment with cross-linking reagents of different lengths ("x" indicates the number of atoms in the linker backbone): MTS-2-MTS (5.2 Å), MTS-4-MTS (7.8 Å), MTS-6-MTS (10.4 Å), MTS-11-O3-MTS (16.9 Å), and MTS-14-O4-MTS (20.8 Å). Mean ± SEM is shown (n = 3–15; some data symbols and error bars are hidden by other data symbols).

ENaC opening, whereas reduced distance favors the closed state. In the next section, we tested this model more directly at the single-channel level.

Cross-linking alters ENaC gating

We tested the effect of cross-linking on ENaC gating by recording single-channel currents (cell-attached patch clamp with Li^+ as the permeant cation to increase the signal to noise ratio). Fig. 6 A shows a representative trace for $\alpha_{K477C}\beta_{V85C}\gamma$ENaC that was not treated with cross-linker; the P_O was 0.40 ± 0.06 (Fig. 6, A and B; and Table 1), similar to wild-type ENaC (Snyder et al., 1995). Treatment with MTS-14-O4-MTS increased ENaC P_O to 0.60 ± 0.04 (Fig. 6, A and B; and Table 1). In contrast, it had no significant effect on single-channel conductance (8.06 ± 0.07 pS without modification [n = 8], 6.51 ± 0.90 pS with modification [n = 5], P = 0.103). Thus, cross-linking by MTS-14-O4-MTS increased current by altering channel gating. However, the increase in P_O was less than we expected, based on the fivefold increase in whole-cell current produced by MTS-14-O4-MTS. Quantitation of ENaC gating is complicated by a high degree of variability in P_O, in part because of differences in the proteolytic cleavage state of individual ENaC channels (Hughey et al., 2003, 2004; Caldwell et al., 2004; Carattino et al., 2008; Kashlan et al., 2012); ENaC activity is enhanced by proteolytic removal of α- and γENaC extracellular domain segments. To reduce variability, we eliminated cleavage of γENaC by mutating its proteolytic cleavage sites, which converts channels to a low-activity state (Carattino et al., 2008). When coexpressed with α_{K477C} and β_{V85C}, P_O was 0.03 ± 0.01 (Fig. 6, C and D; and Table 1). MTS-14-O4-MTS increased P_O fourfold to 0.12 ± 0.02 (Fig. 6, C and D; and Table 1), consistent with the increase in ENaC activity observed at the whole cell level.

We also tested the effect of a short cross-linker, MTS-2-MTS, on ENaC gating. We hypothesized that by reducing intersubunit distance, MTS-2-MTS would decrease ENaC P_O. To facilitate detection of such a change, we exposed the outside of the channel to a low cation concentration (1 mM Li^+ in pipette) to enhance ENaC activity (Bize and Horisberger, 2007) and measured outward current at a holding potential of 60 mV. Under these conditions, the P_O of unmodified channels was high (0.67 ± 0.13; Fig. 6, E and F; and Table 1), and treatment with MTS-2-MTS reduced P_O to 0.20 ± 0.08 (Fig. 6,

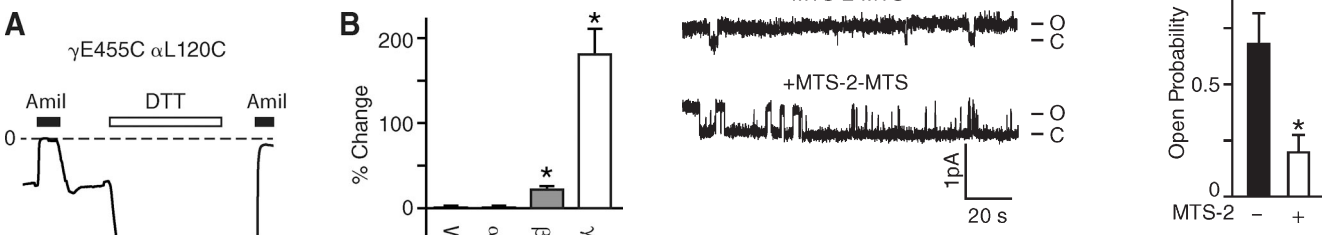

Figure 6. Cross-linking alters ENaC open probability. (A–D) Representative single-channel current traces (cell-attached configuration) obtained at −100 mV (110 mM LiCl in bath and pipette) in oocytes expressing $\alpha_{K477C}\beta_{V85C}\gamma$ENaC (A and B) or $\alpha_{K477C}\beta_{V85C}\gamma_{R135A,\ R137A,\ R138A,\ R178W,\ R179A,\ R180A,\ R181A}$ENaC (C and D) without (top traces) or with (bottom traces) MTS-14-O4-MTS pretreatment. (B) Open probability determined from patches described in A (n = 5–8; *, P < 0.045). (D) Open probability determined from patches described in C (n = 5; *, P < 0.025). (E) Representative single-channel current traces (cell-attached configuration) obtained at 60 mV (110 mM LiCl in bath and 1 mM LiCl in pipette) in oocytes expressing $\alpha_{K477C}\beta_{V85C}\gamma$ENaC without (top trace) or with (bottom trace) MTS-2-MTS pretreatment. (F) Open probability determined from patches described in E (n = 4–7; *, P < 0.015). Mean ± SEM is shown.

Figure 5. Spontaneous disulfide bond reduces ENaC current. (A) Representative current trace (voltage clamped to −60 mV) in a *Xenopus* oocyte expressing $\alpha_{L120C}\beta\gamma_{E455C}$ENaC. Amiloride-sensitive ENaC current was measured before and after treatment with 30 mM DTT (white bar). ENaC current was determined by block with 10 μM amiloride (Amil, black bars). (B) Percent change in ENaC current induced by DTT in oocytes expressing αβγENaC (subunits are wild type or the indicated mutants). Mean ± SEM is shown (n = 6–7; *, P < 0.002).

TABLE 1

ENaC single-channel properties

Construct	*n*	N	t	NP_O	P_O
			min		
$\alpha_{K477C}\beta_{V85C}\gamma$	8	1.9 ± 0.4	8.7 ± 0.6	0.74 ± 0.18	0.40 ± 0.06
$\alpha_{K477C}\beta_{V85C}\gamma$ + MTS-14-O4-MTS	5	1.6 ± 0.2	9.0 ± 0.5	0.98 ± 0.32	0.60 ± 0.09
$\alpha_{K477C}\beta_{V85C}\gamma_{Uncleaved}$	5	1	6.7 ± 0.9	0.03 ± 0.01	0.03 ± 0.01
$\alpha_{K477C}\beta_{V85C}\gamma_{Uncleaved}$ + MTS-14-O4-MTS	5	1.6 ± 0.4	9.3 ± 0.5	0.22 ± 0.11	0.12 ± 0.03
$\alpha_{K477C}\beta_{V85C}\gamma$ Low Li^+	4	1.5 ± 0.3	9.8 ± 0.1	0.92 ± 0.15	0.67 ± 0.13
$\alpha_{K477C}\beta_{V85C}\gamma$ Low Li^+ + MTS-14-O4-MTS	7	1.9 ± 0.4	8.0 ± 1.0	0.46 ± 0.18	0.20 ± 0.08

Values of ENaC single-channel properties shown in Fig. 7, including the number of patches studied (*n*), mean number of channels per patch (N), mean duration of the experiments in minutes (t), mean product of the number of channels per patch, and the estimated open probability (NP_O) and mean estimated channel open probability (P_O). No analyzed patch contained more than three channels.

E and F; and Table 1). Thus, cross-linking with MTS-2-MTS altered ENaC gating by favoring the closed state.

Electrostatic effects at interfaces alter ENaC activity

The opposing effects of short and long cross-linkers on ENaC activity suggest that shortening the distance between interfacing residues favors channel closing, whereas lengthening of the distance favors channel opening. As an additional strategy to assess this model, we tested the effects of electrostatic interactions between the interfacing residues.

We first examined the interface between the positively charged residue α_{K477} and β_{V85}. We replaced β_{V85} with cysteine, coexpressed this subunit with wild-type α- and γENaC in *Xenopus* oocytes, and then acutely varied the charge at this position by covalent modification with MTSET and MTSES (which have no effects on wild-type ENaC [Snyder et al., 1999]). Like charges at the interfacing residues should increase the distance between them through electrostatic repulsion, whereas opposing (attractive) charges should reduce the distance. When we introduced a positively charged side chain, by exposure of oocytes to MTSET, ENaC current was irreversibly increased (Fig. 7, A and C). Thus, like charges increased ENaC activity. Conversely, introduction of a negative charge (MTSES) irreversibly decreased ENaC current (Fig. 7, B and C); opposing charges reduced ENaC activity.

We examined a second intersubunit interface between negatively charged γ_{E455} and α_{L120} (which we replaced with cysteine). In this case, introduction of a positive charge (MTSET) decreased ENaC current, whereas a negative charge (MTSES) increased current (Fig. 7 D). Thus, at both interfaces, repulsive (like) charges increased ENaC activity, whereas attractive (opposite) charges reduced activity. These data support the concept that intersubunit conformational changes contribute to ENaC gating, with movement of the residues farther apart favoring channel opening and movement closer together favoring channel closing.

Cross-linking disrupts ENaC regulation by extracellular pH and Na^+

ENaC gating is modulated by extracellular signals. We tested whether intersubunit conformational changes underlie this regulation by cross-linking interfaces to constrain movements. We first examined ENaC regulation by extracellular pH, which requires acidic residues at two of the interfaces (β_{E446} and γ_{E455}; Collier et al., 2012). To keep these residues intact, we used the interface between α_{K477C} and $\beta_{V85C}\gamma$ to introduce the cross-link. Before

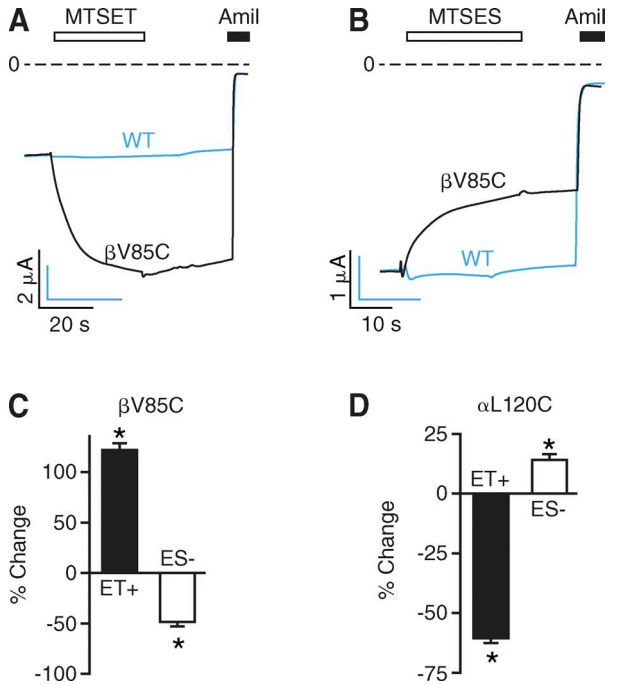

Figure 7. Electrostatic effects at interfaces alter ENaC activity. (A and B) Representative current traces in *Xenopus* oocytes (voltage clamped to −60 mV) expressing wild-type ENaC (blue) or $\alpha\beta_{V85C}\gamma$ENaC (black) treated with MTSET (white bar, A) or MTSES (white bar, B). ENaC current was determined by block with 10 μM amiloride (Amil, black bars). (C and D) Percent change in ENaC current after treatment with MTSET (ET+) or MTSES (ES−) for cells expressing $\alpha\beta_{V85C}\gamma$ENaC (C) or $\alpha_{L120C}\beta\gamma$ENaC (D). Mean ± SEM is shown ($n = 12$; *, $P < 0.0002$).

cross-linking, acidic extracellular solution increased amiloride-sensitive current (Fig. 8, A and B), whereas alkaline pH reduced current (Fig. 8 B). After treatment with MTS-14-O4-MTS, there was a large decrease in ENaC stimulation by acidic pH (Fig. 8, A and B; traces were scaled to facilitate comparison of pH responses) and a smaller decrease in inhibition by alkaline pH (Fig. 8 B). MTS-2-MTS had a similar effect (Fig. 8 B). Thus, cross-linking disrupted ENaC regulation by pH, implicating a critical role for intersubunit conformational changes.

ENaC activity is also regulated by extracellular Na^+ through a negative feedback mechanism known as Na^+ self-inhibition. To test whether intersubunit conformational changes are also required for this process, we asked if it would be disrupted by cross-linking. We began by examining the pairing of α_{L120C} and γ_{E455C}, which form a spontaneous disulfide bond. We incubated ENaC in low extracellular Na^+ (1 mM; Fig. 9 A), which converts ENaC to a high P_O state (Chraïbi and Horisberger, 2002). We then rapidly shifted to a high-Na^+ (116 mM) solution, generating a large peak in Na^+ current (Fig. 9 A, red lines) that decreased over time to a lower steady-state level (Fig. 9 A, blue lines). This decrease in current reflects the degree to which ENaC is inhibited by extracellular Na^+. When cells expressed $\alpha_{L120C}\beta\gamma_{E455C}$ENaC, DTT increased the fraction of current inhibited by Na^+ by 35 ± 8% (Fig. 9, A and B). DTT had no effect on Na^+ self-inhibition for wild-type ENaC or channels with cysteines at the other two interfaces (Fig. 9 B). These data suggest that spontaneous cross-linking of α_{L120C} and γ_{E455C} disrupts conformational changes required for ENaC Na^+ self-inhibition.

We interrogated the interface between α_{K477C} and β_{V85C} using bifunctional cysteine-reactive reagents. In cells expressing $\alpha_{K477C}\beta_{V85C}\gamma$ENaC, MTS-14-O4-MTS reduced Na^+ self-inhibition by 37.7 ± 3.3% (Fig. 9, C, D, and G). In contrast, MTS-14-O4-MTS did not reduce Na^+ self-inhibition for wild-type ENaC or for ENaC containing a single cysteine substitution (α_{K477C} or β_{V85C}; Fig. 9 G). Thus, cross-linking α_{K477} and β_{V85} with MTS-14-O4-MTS reduced Na^+ self-inhibition.

In Fig. 9 (E–G), we tested the effect of the shorter cross-linker MTS-2-MTS on Na^+ self-inhibition. In cells expressing $\alpha_{K477C}\beta_{V85C}\gamma$ENaC, MTS-2-MTS produced a large decrease in Na^+ self-inhibition (74.6 ± 6.9%), much greater than the effects of MTS-2-MTS on wild-type ENaC or the single cysteine mutants (Fig. 9 G). This resulted from a decrease in the peak current elicited by addition of Na^+ to the extracellular solution. Similarly, MTS-4-MTS, MTS-6-MTS, and MTS-11-O3-MTS also decreased Na^+ self-inhibition (Fig. 9 G). Thus, reagents with a wide range of lengths were capable of cross-linking cysteines at the interface between α_{K477} and β_{V85}. Although only the relatively long cross-linkers were sufficient to increase ENaC current, cross-linkers reduced Na^+ self-inhibition independent of their length. By constraining movements at this interface, cross-linking likely disrupts ENaC transitions between the open and closed states.

DISCUSSION

This work elucidates a mechanism that mediates ENaC gating. We found that conformational changes at interfaces located between the three ENaC subunits participate in the transition between the open and closed states (illustrated in Fig. 10). Movements that increase the distance between interfacing residues favor channel opening, an effect mimicked by introduction of long cross-linkers or repulsive charges. Conversely, movements that shorten intersubunit distances favor ENaC closing, a state mimicked by short cross-linkers or attractive charges. Thus, the interfaces between ENaC subunits are important locations for the regulation of ENaC gating.

The data allow us to estimate the minimum distances between the interfacing residues. MTS-2-MTS cross-linked α_{K477C} to β_{V85C} and β_{E446C} to γ_{V87C}, indicating that the sulfur atoms within these residue pairs are located within 5 Å of one another. The distance between γE455C and αL120C is ≤2 Å based on their ability to form a spontaneous disulfide bond. These reflect the intersubunit distances when the channel is closed. In the open state, the intersubunit distances increase. At the interface between α_{K477C} and β_{V85C}, only cross-linkers 16.9 Å or longer were sufficient to increase ENaC activity. The actual intersubunit distance in the open state may be

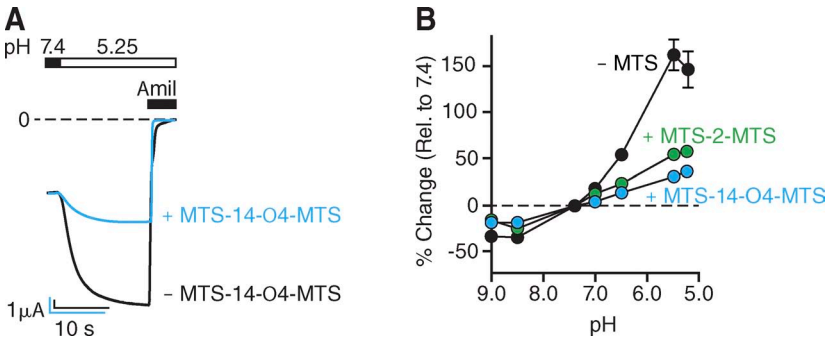

Figure 8. Cross-linking disrupts pH regulation. (A) Representative current traces in *Xenopus* oocytes (voltage clamped to −60 mV) expressing $\alpha_{K477C}\beta_{V85C}\gamma$ENaC before (black, −MTS-14) and after (blue, +MTS-14) treatment with MTS-14-O4-MTS. Extracellular pH was shifted from 7.4 to 5.25, as indicated. The two traces were obtained from different cells and are scaled to facilitate comparisons. (B) Percent change in ENaC current (relative to current at pH 7.4) in response to changes in extracellular pH before (black) and after treatment with MTS-14-O4-MTS (blue) or MTS-2-MTS (green). Mean ± SEM is shown (n = 3–6; some data symbols and error bars are hidden by other data symbols).

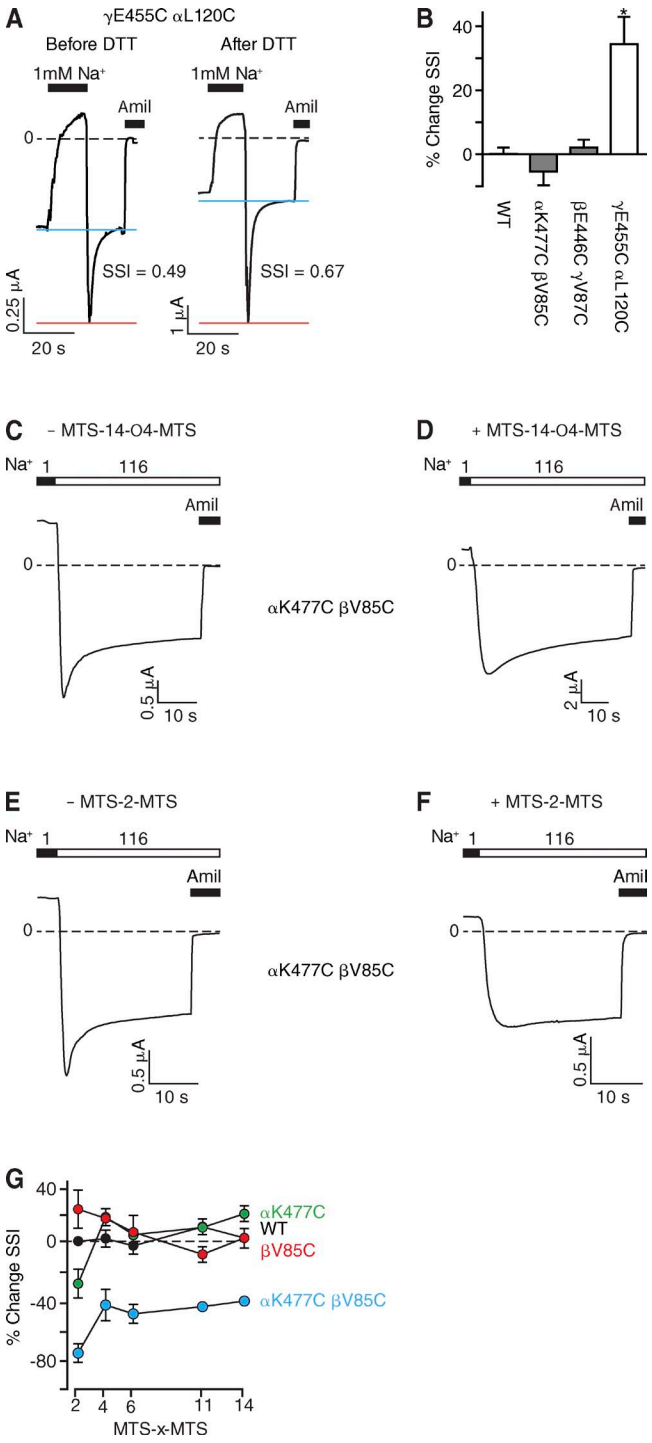

Figure 9. Cross-linking decreases Na^+ self-inhibition. (A) Representative current traces in *Xenopus* oocytes (voltage clamped to −60 mV) expressing $\alpha_{L120C}\beta\gamma_{E455C}$ENaC, before and after treatment with 30 mM DTT for 30 s. To quantitate Na^+ self-inhibition, extracellular Na^+ was transiently reduced to 1 mM, as indicated by the black bar, and then rapidly shifted back to 116 mM Na^+. ENaC current was blocked by 10 μM amiloride (Amil, black bar). (B) Percent change in Na^+ self-inhibition (SSI) induced by DTT in oocytes expressing αβγENaC (subunits are wild type or the indicated mutants). Mean ± SEM is shown (n = 6–7; *, P < 0.005). (C–F) Representative current traces in oocytes (voltage clamped to −60 mV) expressing $\alpha_{K477C}\beta_{V85C}\gamma$ENaC before (C and E) and after (D and F) treatment with MTS-14-O4-MTS or MTS-2-MTS. The extracellular solution contained 1 mM Na^+ (black bar) or 116 mM Na^+ (white bar). (G) Percent change in Na^+ self-inhibition (SSI) for cells expressing αβγ (black), $\alpha_{K477C}\beta\gamma$ (green), $\alpha\beta_{V85C}\gamma$ (red), or $\alpha_{K477C}\beta_{V85C}\gamma$ENaC (blue) induced by treatment with cross-linking reagents of different lengths (MTS-x-MTS, where "x" indicates the number of atoms in the linker backbone). Mean ± SEM is shown (n = 3–15; some error bars are hidden by data symbols).

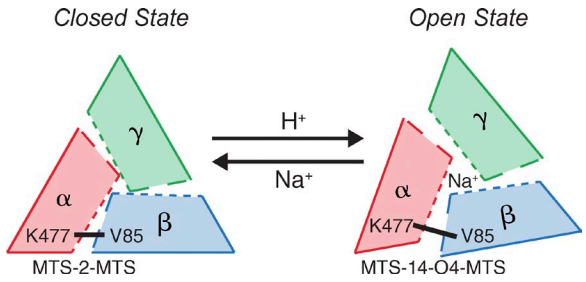

Figure 10. ENaC gating model. Two state model of heterotrimeric ENaC as viewed from the top of the channel. Each subunit is represented as an irregular trapezoid. Approximate location of α_{K477} and β_{V85} are indicated on the model. Cross-linking with MTS-2-MTS favors the ENaC closed state and MTS-14-O4-MTS favors the open state. ENaC gating is regulated by extracellular protons (stimulatory) and Na^+ (inhibitory); cross-linking disrupted this regulation by preventing transitions between the open and closed states.

shorter than this because the cross-linkers are flexible (Zhou et al., 2008). However, they are likely to push apart the interfacing residues through the bulk of their long spacers. Importantly, our conclusions are supported by a second strategy using electrostatic repulsive and attractive effects to alter intersubunit distance.

The interfaces we identified play key roles in ENaC regulation by protons. Acidic residues at two of the three interfaces are required for protons to increase ENaC activity, likely by functioning as protonation sites (Collier et al., 2012). We speculate that protonation drives conformational changes that increase intersubunit distances through an electrostatic process, similar to the effects of long cross-linkers and repulsive charges. However, the ENaC homology model does not provide sufficient resolution to identify the potential charged interaction partners for these residues.

In addition to their role in pH regulation, interfaces between ENaC subunits contribute to modulation by other extracellular ions. For example, we found that constraining movements between interfacing residues (by cross-linking) disrupted ENaC inhibition by Na^+. Both short and long cross-linkers reduced Na^+ self-inhibition, presumably by preventing the channel from transitioning between open and closed conformations. Thus, conformational changes at the intersubunit interfaces are required for ENaC Na^+ self-inhibition. In previous work, we identified two Cl^- binding sites at a different location between adjacent subunits. Binding of Cl^- to

one interface (α-β) inhibits ENaC activity by increasing Na^+ self-inhibition, whereas Cl^- binding to the second interface (β-γ) inhibits ENaC in an Na^+-independent manner (Collier and Snyder, 2011). External Cu^{2+} also inhibits ENaC at interfaces between the ENaC subunits (Chen et al., 2011). Thus, the interfaces harbor binding sites that allow ENaC to respond to a variety of extracellular modulators. In other channels, intersubunit interfaces have a similar function. For example, ligand-gated channels including the acetylcholine receptor and glycine receptor are activated through agonist binding to interfaces between adjacent subunits (Czajkowski et al., 1993; Czajkowski and Karlin, 1995; Todorovic et al., 2010). Activity of kainate subtype glutamate receptors is modulated by binding of Na^+ and Cl^- to dimer interfaces in the extracellular domain (Chaudhry et al., 2009).

Our data indicate that movements at all three intersubunit interfaces contribute to ENaC gating. However, it is interesting that there is asymmetry between them. First, there are charge differences. Two of the sites contain negatively charged residues (β_{E446} and γ_{E455}) that function as putative proton sensors, whereas the third interface contains a positively charged residue (α_{K477}). Second, a spontaneous disulfide bond formed between γ_{E455C} and α_{L120C} but did not occur at the other two interfaces. This suggests differences in the minimum distances between residues at the three interfaces. Third, although cross-linking each interface with MTS-14-O4-MTS increased ENaC activity, there were quantitative differences; cross-linking β_{E446C} to γ_{V87C} increased current much less than cross-linking the other two interfaces. It is not yet clear whether movements occur at all three interfaces in a concerted manner or whether movements at a single interface are sufficient to modulate ENaC gating.

It is also not yet clear how movements at the interfaces are transduced into changes in ENaC gating. Previous work implicated movements in the outer vestibule at the DEG residue, named because an equivalent mutation in a related channel (MEC-4) causes neurodegeneration in *Caenorhabditis elegans* (Driscoll and Chalfie, 1991). Bulky or charged residues at this location lock ENaC in an open state, and accessibility to its side chain is state dependent, occurring selectively in the open state (Snyder et al., 2000). Similar movements at this location occur in ASICs (Adams et al., 1998; Tolino et al., 2011). Recently, chicken ASIC1a was crystallized in putative open states, bound to psalmotoxin 1 (PDB IDs 4FZ0 and 4FZ1; Baconguis and Gouaux, 2012) and to snake toxin (4NTW; Baconguis et al., 2014). Both toxins produce small constitutive currents. Toxin binding induced lateral movements in the palm domain β1–β2 linkers (location of α_{L120}, β_{V85}, and γ_{V87} in ENaC), which were transduced into transmembrane domain movements thought to open the channel pore (Baconguis and Gouaux, 2012; Baconguis et al., 2014). Importantly, in the putative open (toxin bound) states, there was an increase in the distance between intersubunit interface residues (Met 364 and Val 81) equivalent to those we identified in ENaC. Although it is not known whether the structures of the toxin-bound ASIC1a reflect conformational changes that occur during physiological activation or whether gating-associated conformation changes are conserved between ENaC and ASIC1, the data support the concept that movements at the intersubunit interfaces contribute to gating of DEG/ENaC ion channels.

Other extracellular domain regions have also been implicated in ENaC gating. Proteolytic cleavage releases inhibitory segments from α- and γENaC, which increases ENaC activity. Elegant structural modeling of αENaC suggests that the inhibitory segment constrains gating motions at a location between the thumb and finger domains (Kashlan et al., 2011, 2012). Gating is also disrupted by mutations at the base of the thumb domain (Shi et al., 2011), in the finger domain (Shi et al., 2012a), and in the wrist domain (Shi et al., 2012b). Additional work will be necessary to determine whether these regions function coordinately with the intersubunit interfaces or whether they alter ENaC gating through independent mechanisms.

ENaC is a constitutively active channel, but a wide variety of extracellular stimuli can modulate its activity. In the collecting duct and connecting tubule of the kidney, ENaC is exposed to extreme changes in the concentrations of H^+, Na^+, and Cl^- during changes in volume status and diet. The ENaC extracellular domain functions as a sensor to detect changes in the composition of the highly variable extracellular milieu in which ENaC resides. We speculate that this rapid tuning of channel activity in response to changing extracellular conditions may allow ENaC to respond to a variety of challenges that threaten to disrupt Na^+ transport and fluid homeostasis. Conformational changes at intersubunit interfaces play a critical role in this regulation and provide an attractive site to target pharmacological modulation of Na^+ absorption.

We thank Diane Olson and Abigail Hamilton for assistance and acknowledge the University of Iowa DNA Core Facility for reagents and DNA sequencing.

P.M. Snyder was supported by National Institutes of Health grant HL072256 and Veterans Affairs grant BX001862, D.M. Collier by a predoctoral fellowship from the American Heart Association (10PRE2610282) and National Institutes of Health grant 2T32HL007121-36, and C.J. Benson by Veterans Affairs grant BX000776.

The authors declare no competing financial interests.

Lawrence G. Palmer served as editor.

Submitted: 10 April 2014
Accepted: 14 August 2014

REFERENCES

Adams, C.M., P.M. Snyder, M.P. Price, and M.J. Welsh. 1998. Protons activate brain Na^+ channel 1 by inducing a conformational change that exposes a residue associated with neurodegeneration. *J. Biol. Chem.* 273:30204–30207. http://dx.doi.org/10.1074/jbc.273.46.30204

Baconguis, I., and E. Gouaux. 2012. Structural plasticity and dynamic selectivity of acid-sensing ion channel-spider toxin complexes. *Nature.* 489:400–405. http://dx.doi.org/10.1038/nature11375

Baconguis, I., C.J. Bohlen, A. Goehring, D. Julius, and E. Gouaux. 2014. X-ray structure of acid-sensing ion channel 1-snake toxin complex reveals open state of a Na^+-selective channel. *Cell.* 156: 717–729. http://dx.doi.org/10.1016/j.cell.2014.01.011

Ben-Shahar, Y. 2011. Sensory functions for degenerin/epithelial sodium channels (DEG/ENaC). *Adv. Genet.* 76:1–26. http://dx.doi.org/10.1016/B978-0-12-386481-9.00001-8

Bize, V., and J.D. Horisberger. 2007. Sodium self-inhibition of human epithelial sodium channel: selectivity and affinity of the extracellular sodium sensing site. *Am. J. Physiol. Renal Physiol.* 293: F1137–F1146.

Boucher, R.C., M.J. Stutts, M.R. Knowles, L. Cantley, and J.T. Gatzy. 1986. Na+ transport in cystic fibrosis respiratory epithelia. Abnormal basal rate and response to adenylate cyclase activation. *J. Clin. Invest.* 78:1245–1252. http://dx.doi.org/10.1172/JCI112708

Caldwell, R.A., R.C. Boucher, and M.J. Stutts. 2004. Serine protease activation of near-silent epithelial Na^+ channels. *Am. J. Physiol. Cell Physiol.* 286:C190–C194.

Carattino, M.D., S. Sheng, and T.R. Kleyman. 2004. Epithelial Na^+ channels are activated by laminar shear stress. *J. Biol. Chem.* 279:4120–4126. http://dx.doi.org/10.1074/jbc.M311783200

Carattino, M.D., R.P. Hughey, and T.R. Kleyman. 2008. Proteolytic processing of the epithelial sodium channel γ subunit has a dominant role in channel activation. *J. Biol. Chem.* 283:25290–25295. http://dx.doi.org/10.1074/jbc.M803931200

Chaudhry, C., A.J. Plested, P. Schuck, and M.L. Mayer. 2009. Energetics of glutamate receptor ligand binding domain dimer assembly are modulated by allosteric ions. *Proc. Natl. Acad. Sci. USA.* 106:12329–12334. http://dx.doi.org/10.1073/pnas.0904175106

Chen, J., M.M. Myerburg, C.J. Passero, K.L. Winarski, and S. Sheng. 2011. External Cu^{2+} inhibits human epithelial Na^+ channels by binding at a subunit interface of extracellular domains. *J. Biol. Chem.* 286:27436–27446. http://dx.doi.org/10.1074/jbc.M111.232058

Chraïbi, A., and J.D. Horisberger. 2002. Na self inhibition of human epithelial Na channel: temperature dependence and effect of extracellular proteases. *J. Gen. Physiol.* 120:133–145.

Collier, D.M., and P.M. Snyder. 2009a. Extracellular chloride regulates the epithelial sodium channel. *J. Biol. Chem.* 284:29320–29325. http://dx.doi.org/10.1074/jbc.M109.046771

Collier, D.M., and P.M. Snyder. 2009b. Extracellular protons regulate human ENaC by modulating Na^+ self-inhibition. *J. Biol. Chem.* 284:792–798. http://dx.doi.org/10.1074/jbc.M806954200

Collier, D.M., and P.M. Snyder. 2011. Identification of epithelial Na^+ channel (ENaC) intersubunit Cl- inhibitory residues suggests a trimeric alpha gamma beta channel architecture. *J. Biol. Chem.* 286:6027–6032. http://dx.doi.org/10.1074/jbc.M110.198127

Collier, D.M., Z.J. Peterson, I.O. Blokhin, C.J. Benson, and P.M. Snyder. 2012. Identification of extracellular domain residues required for epithelial Na^+ channel activation by acidic pH. *J. Biol. Chem.* 287:40907–40914. http://dx.doi.org/10.1074/jbc.M112.417519

Czajkowski, C., and A. Karlin. 1995. Structure of the nicotinic receptor acetylcholine-binding site. Identification of acidic residues in the δ subunit within 0.9 nm of the α subunit-binding site disulfide. *J. Biol. Chem.* 270:3160–3164.

Czajkowski, C., C. Kaufmann, and A. Karlin. 1993. Negatively charged amino acid residues in the nicotinic receptor delta subunit that contribute to the binding of acetylcholine. *Proc. Natl. Acad. Sci. USA.* 90:6285–6289. http://dx.doi.org/10.1073/pnas.90.13.6285

Dawson, R.J., J. Benz, P. Stohler, T. Tetaz, C. Joseph, S. Huber, G. Schmid, D. Hügin, P. Pflimlin, G. Trube, et al. 2012. Structure of the acid-sensing ion channel 1 in complex with the gating modifier Psalmotoxin 1. *Nat. Commun.* 3:936. http://dx.doi.org/10.1038/ncomms1917

Driscoll, M., and M. Chalfie. 1991. The *mec-4* gene is a member of a family of *Caenorhabditis elegans* genes that can mutate to induce neuronal degeneration. *Nature.* 349:588–593. http://dx.doi.org/10.1038/349588a0

Garty, H., and L.G. Palmer. 1997. Epithelial sodium channels: function, structure, and regulation. *Physiol. Rev.* 77:359–396.

Gonzales, E.B., T. Kawate, and E. Gouaux. 2009. Pore architecture and ion sites in acid-sensing ion channels and P2X receptors. *Nature.* 460:599–604. http://dx.doi.org/10.1038/nature08218

Hughey, R.P., G.M. Mueller, J.B. Bruns, C.L. Kinlough, P.A. Poland, K.L. Harkleroad, M.D. Carattino, and T.R. Kleyman. 2003. Maturation of the epithelial Na^+ channel involves proteolytic processing of the α- and γ-subunits. *J. Biol. Chem.* 278:37073–37082. http://dx.doi.org/10.1074/jbc.M307003200

Hughey, R.P., J.B. Bruns, C.L. Kinlough, K.L. Harkleroad, Q. Tong, M.D. Carattino, J.P. Johnson, J.D. Stockand, and T.R. Kleyman. 2004. Epithelial sodium channels are activated by furin-dependent proteolysis. *J. Biol. Chem.* 279:18111–18114. http://dx.doi.org/10.1074/jbc.C400080200

Hunt, J. 2007. Exhaled breath condensate pH assays. *Immunol. Allergy Clin. North Am.* 27:597–606. http://dx.doi.org/10.1016/j.iac.2007.09.006

Jasti, J., H. Furukawa, E.B. Gonzales, and E. Gouaux. 2007. Structure of acid-sensing ion channel 1 at 1.9 Å resolution and low pH. *Nature.* 449:316–323. http://dx.doi.org/10.1038/nature06163

Kashlan, O.B., J.L. Adelman, S. Okumura, B.M. Blobner, Z. Zuzek, R.P. Hughey, T.R. Kleyman, and M. Grabe. 2011. Constraint-based, homology model of the extracellular domain of the epithelial Na^+ channel α subunit reveals a mechanism of channel activation by proteases. *J. Biol. Chem.* 286:649–660. http://dx.doi.org/10.1074/jbc.M110.167098

Kashlan, O.B., B.M. Blobner, Z. Zuzek, M.D. Carattino, and T.R. Kleyman. 2012. Inhibitory tract traps the epithelial Na^+ channel in a low activity conformation. *J. Biol. Chem.* 287:20720–20726. http://dx.doi.org/10.1074/jbc.M112.358218

Kelley, L.A., and M.J. Sternberg. 2009. Protein structure prediction on the Web: a case study using the Phyre server. *Nat. Protoc.* 4:363–371. http://dx.doi.org/10.1038/nprot.2009.2

Lifton, R.P. 1996. Molecular genetics of human blood pressure variation. *Science.* 272:676–680. http://dx.doi.org/10.1126/science.272.5262.676

Loo, T.W., and D.M. Clarke. 2001. Determining the dimensions of the drug-binding domain of human P-glycoprotein using thiol cross-linking compounds as molecular rulers. *J. Biol. Chem.* 276: 36877–36880. http://dx.doi.org/10.1074/jbc.C100467200

McDonald, F.J., P.M. Snyder, P.B. McCray Jr., and M.J. Welsh. 1994. Cloning, expression, and tissue distribution of a human amiloride-sensitive Na+ channel. *Am. J. Physiol.* 266:L728–L734.

McDonald, F.J., M.P. Price, P.M. Snyder, and M.J. Welsh. 1995. Cloning and expression of the beta- and gamma-subunits of the human epithelial sodium channel. *Am. J. Physiol.* 268:C1157–C1163.

Morimoto, T., W. Liu, C. Woda, M.D. Carattino, Y. Wei, R.P. Hughey, G. Apodaca, L.M. Satlin, and T.R. Kleyman. 2006. Mechanism underlying flow stimulation of sodium absorption in the mammalian collecting duct. *Am. J. Physiol. Renal Physiol.* 291:F663–F669.

Pettersen, E.F., T.D. Goddard, C.C. Huang, G.S. Couch, D.M. Greenblatt, E.C. Meng, and T.E. Ferrin. 2004. UCSF Chimera—a visualization system for exploratory research and analysis. *J. Comput. Chem.* 25:1605–1612. http://dx.doi.org/10.1002/jcc.20084

Pezzulo, A.A., X.X. Tang, M.J. Hoegger, M.H. Alaiwa, S. Ramachandran, T.O. Moninger, P.H. Karp, C.L. Wohlford-Lenane, H.P. Haagsman, M. van Eijk, et al. 2012. Reduced airway surface pH impairs bacterial killing in the porcine cystic fibrosis lung. *Nature.* 487:109–113. http://dx.doi.org/10.1038/nature11130

Rose, B.D. 1984. Clinical Physiology of Acid-Base and Electrolyte Disorders. Second edition. McGraw-Hill, New York. 702 pp.

Schild, L. 2004. The epithelial sodium channel: from molecule to disease. *Rev. Physiol. Biochem. Pharmacol.* 151:93–107. http://dx.doi.org/10.1007/s10254-004-0023-7

Sheng, S., J.B. Bruns, and T.R. Kleyman. 2004. Extracellular histidine residues crucial for Na^+ self-inhibition of epithelial Na^+ channels. *J. Biol. Chem.* 279:9743–9749. http://dx.doi.org/10.1074/jbc.M311952200

Shi, S., D.D. Ghosh, S. Okumura, M.D. Carattino, O.B. Kashlan, S. Sheng, and T.R. Kleyman. 2011. Base of the thumb domain modulates epithelial sodium channel gating. *J. Biol. Chem.* 286:14753–14761. http://dx.doi.org/10.1074/jbc.M110.191734

Shi, S., B.M. Blobner, O.B. Kashlan, and T.R. Kleyman. 2012a. Extracellular finger domain modulates the response of the epithelial sodium channel to shear stress. *J. Biol. Chem.* 287:15439–15444. http://dx.doi.org/10.1074/jbc.M112.346551

Shi, S., M.D. Carattino, and T.R. Kleyman. 2012b. Role of the wrist domain in the response of the epithelial sodium channel to external stimuli. *J. Biol. Chem.* 287:44027–44035. http://dx.doi.org/10.1074/jbc.M112.421743

Snyder, P.M. 2005. Minireview: regulation of epithelial Na^+ channel trafficking. *Endocrinology.* 146:5079–5085. http://dx.doi.org/10.1210/en.2005-0894

Snyder, P.M., M.P. Price, F.J. McDonald, C.M. Adams, K.A. Volk, B.G. Zeiher, J.B. Stokes, and M.J. Welsh. 1995. Mechanism by which Liddle's syndrome mutations increase activity of a human epithelial Na^+ channel. *Cell.* 83:969–978. http://dx.doi.org/10.1016/0092-8674(95)90212-0

Snyder, P.M., D.R. Olson, and D.B. Bucher. 1999. A pore segment in DEG/ENaC Na^+ channels. *J. Biol. Chem.* 274:28484–28490. http://dx.doi.org/10.1074/jbc.274.40.28484

Snyder, P.M., D.B. Bucher, and D.R. Olson. 2000. Gating induces a conformational change in the outer vestibule of ENaC. *J. Gen. Physiol.* 116:781–790. http://dx.doi.org/10.1085/jgp.116.6.781

Todorovic, J., B.T. Welsh, E.J. Bertaccini, J.R. Trudell, and S.J. Mihic. 2010. Disruption of an intersubunit electrostatic bond is a critical step in glycine receptor activation. *Proc. Natl. Acad. Sci. USA.* 107:7987–7992. http://dx.doi.org/10.1073/pnas.1001845107

Tolino, L.A., S. Okumura, O.B. Kashlan, and M.D. Carattino. 2011. Insights into the mechanism of pore opening of acid-sensing ion channel 1a. *J. Biol. Chem.* 286:16297–16307. http://dx.doi.org/10.1074/jbc.M110.202366

Zhou, Y., L. Guan, J.A. Freites, and H.R. Kaback. 2008. Opening and closing of the periplasmic gate in lactose permease. *Proc. Natl. Acad. Sci. USA.* 105:3774–3778. http://dx.doi.org/10.1073/pnas.0800825105